

Reconstructions and origin of surface states on AlN polar and nonpolar surfaces

M. S. Miao, A. Janotti, and C. G. Van de Walle

Materials Department, University of California, Santa Barbara, California 93106-5050, USA

(Received 13 July 2009; revised manuscript received 3 September 2009; published 19 October 2009)

The AlN (0001), (000 $\bar{1}$), (10 $\bar{1}0$), and (11 $\bar{2}0$) surfaces and their electronic structures are studied based on density-functional theory using the generalized gradient approximation as well as the hybrid functional approach. The stable reconstructions generally satisfy the electron-counting rule, except for cases where Al adlayers are present. We find that the transitions between different reconstructions exhibit a distinct trend for group-III nitrides. For all surfaces, Al dangling-bond states tend to be close to the conduction-band minimum (CBM) and N dangling-bond states close to the valence-band maximum (VBM). Al-N bonding states also occur near the VBM, while Al-Al bonding states occur in the middle of the gap. We find that Al dangling-bond states on the Al-polar (0001) surface can pin the Fermi level of *n*-type AlN at 1.0 eV below the CBM at moderate Al/N growth ratios. At high Al/N ratios, metallic Al adlayers form which pin the Fermi level in the middle of the gap. The lack of a surface donor state in the upper part of the gap suggests that the surface states on clean AlGa_xN surfaces are unlikely to be the source of carriers in the two-dimensional electron gas in AlGa_xN/GaN high-electron-mobility transistors.

DOI: [10.1103/PhysRevB.80.155319](https://doi.org/10.1103/PhysRevB.80.155319)

PACS number(s): 68.47.Fg, 68.35.Md, 73.20.At

I. INTRODUCTION

Among group-III nitride semiconductors, AlN has the largest band gap (6.2 eV). Since its lattice parameters are close to GaN, high-quality AlGa_xN and AlInGa_xN materials can be synthesized over a large range of Al compositions, providing a unique way of engineering the electronic structure through alloying. These materials have received intensive attention for application in optoelectronic devices as well as high-power and high-frequency electronic devices.¹⁻⁵

Surface reconstructions play an important role in crystal quality and therefore also device performance, because they can significantly affect the morphology as well as the defect and impurity incorporation. Detailed knowledge of atomic structure of the surfaces under growth conditions greatly aids in producing high-quality epitaxial layers.⁶⁻⁸ Nitride films for devices have usually been grown along the (0001) direction, resulting in large polarization fields that separate the electrons and the holes in light-emitting devices and lower their efficiencies. Recently, considerable effort has been invested in fabricating optoelectronic devices along nonpolar orientations,⁹⁻¹² thus eliminating the effects of polarization fields and increasing the efficiency of light emission. Understanding surface reconstructions on both polar and nonpolar surfaces is therefore important.

Surface reconstructions also affect the electronic structure of the surface and therefore the performance of electronic and optoelectronic devices. In some cases, such as AlGa_xN/GaN high-electron-mobility transistors (HEMTs), surface states have been proposed to be the source of the two-dimensional electron gas (2DEG) at the AlGa_xN/GaN interface.¹³⁻¹⁶ A number of experiments, including those measuring the dependence of carrier density on AlGa_xN layer thickness, located the position of the relevant surface states in the upper part of the band gap, for example, at 1.65 eV below the conduction-band minimum (CBM) for Al_{0.34}Ga_{0.66}N.¹³ However, the microscopic origin of such surface states has not yet been determined.

A number of theoretical studies have been conducted for AlN surfaces,^{8,17-20} including first-principles calculations of AlN polar^{8,17-20} and nonpolar¹⁸ surfaces. However, because of the underestimation of band gaps in calculations based on density-functional theory (DFT) in the local-density approximation (LDA) or generalized gradient approximation (GGA), large uncertainties remain regarding the calculated positions of surface states. More recently,²¹⁻²⁴ the atomic and electronic structures of GaN and InN surfaces were investigated by the use of a modified pseudopotential approach²⁵ that can provide band gaps comparable to experimental values. The surface states that are responsible for pinning the Fermi level on the surfaces of *n*- and *p*-type materials were identified, and their locations were in good agreement with available experimental results. It would be illuminating to further examine the atomic and electronic structure of AlN and compare the results with GaN and InN. Moreover, because the band-gap bowing in AlGa_xN alloys is quite small, a linear interpolation between AlN and GaN is expected to be a good approximation for locating surface states of AlGa_xN alloys.

In the present study, we investigate the reconstructions of polar and nonpolar surfaces of AlN including (0001) (+*c* plane), (000 $\bar{1}$) ($-c$ plane), (10 $\bar{1}0$) (*m* plane), and (11 $\bar{2}0$) (*a* plane) surfaces and their effects on electronic structure. The computational methods will be briefly described in Sec. II. Section III will present results and discussion for the atomic and electronic structure of the surfaces. We will make some concluding remarks in Sec. IV.

II. METHODOLOGY

Our calculations are based on DFT.^{26,27} It is well known that DFT using the LDA or the GGA generates band gaps that are too small in comparison with experimental values. This underestimation of the band gap is particularly problematic in the case of surface calculations because the posi-

tion of surface states in the gap is obtained directly from the Kohn-Sham levels.²⁷ In previous studies for GaN and InN surfaces, we employed a modified pseudopotential²⁵ approach in which a highly localized repulsive potential is inserted at the center of each ion.²⁸ This potential shifts the energy of s orbitals and therefore increases the band gap because the states around the CBM are usually dominated by cation s orbitals. Our attempts to apply this approach to AlN encountered difficulties. Because of the relatively low energies of conduction bands at the K and L points in the Brillouin zone, the band gap tends to become indirect when the CBM at the Γ point is shifted upward by adding a repulsive potential that shifts s orbitals. We therefore had to identify a different methodology to address band-gap errors. Fortunately, AlN contains no d electrons and lends itself more easily to computationally more intensive approaches, for instance, those that employ exchange-correlation methods involving the calculation of the Hartree-Fock (HF) exchange energy, as in hybrid functional methods. As demonstrated recently for In pnictides,²⁹ the hybrid functional not only corrects the band gap, but actually changes the dispersion of bands, resulting, e.g., in more accurate effective masses.

In this work, we employ the Perdew-Burke-Ernzerhof (PBE) (Ref. 30) version of GGA to calculate the atomic structure of surface reconstructions on AlN polar and nonpolar surfaces. The electronic structure of the resulting energetically favorable reconstructions is then studied using a hybrid functional approach implemented in the framework of Heyd-Scuseria-Ernzerhof (HSE).^{31–33} For the ionic potential, we use projected augmented wave potentials.^{34,35} All the calculations are performed using the VASP code.^{36,37}

The HSE hybrid functional with standard, i.e., 25% mixing of HF produces a direct band-gap value of 5.7 eV for AlN, which is about 0.4–0.5 eV lower than the experimental values of 6.19 eV (Ref. 38) and 6.12 eV.³⁹ By increasing the mixing parameter to 32%, we obtained a gap of 6.1 eV. This value is in good agreement with the experimental results^{38,39} and the recent GW calculations.⁴⁰ Extensive test calculations were performed for bulk AlN using both the GGA and the hybrid functional with 32% mixing. Both approaches generate reliable lattice parameters. With GGA we obtain $a=3.116$ Å, $c/a=1.604$, and $u=0.382$; HSE with 32% mixing yields $a=3.096$ Å, $c/a=1.601$, and $u=0.381$. These values are in very good agreement with experiment: $a=3.11$ Å, $c/a=1.601$, and $u=0.382$.^{41,42} The close agreement between GGA and HSE also justifies our computational procedure of optimizing the atomic structures using GGA and then using the HSE to calculate the electronic structure.

Supercell slab models are employed to calculate the surface reconstructions. For polar surface calculations, slabs of up to eight AlN bilayers in a (2×2) surface unit cell with a vacuum thickness corresponding to four bilayers (~ 10.0 Å) are used. For nonpolar surfaces, the slab models contain eight AlN bilayers and are separated by a vacuum corresponding to eight bilayers (~ 10.7 Å). A $4 \times 4 \times 1$ k -point mesh is used for most of the calculations, and a cut-off energy of 400 eV ensures the convergence of forces and energies for all surface reconstructions, some of which exhibit very different types of chemical bonding.

To compare the relative stability of various surface reconstructions, we calculated the formation energy $\Delta E^f(\mu_{\text{Al}})$ as a

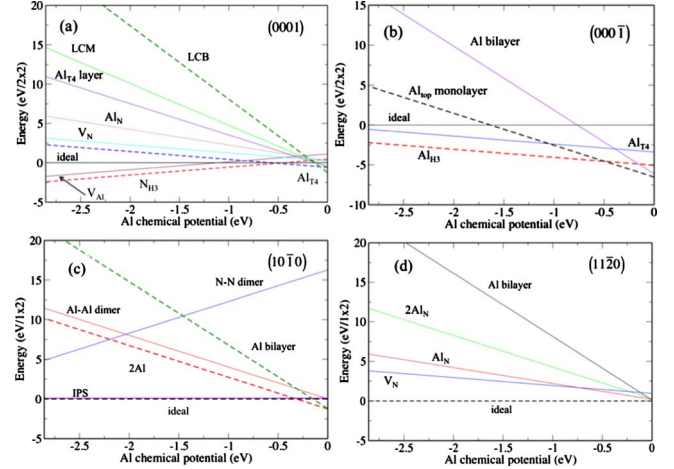


FIG. 1. (Color online) Calculated energies of surface reconstructions on AlN polar and nonpolar surfaces as a function of Al chemical potential. (a) Al polar (0001) surface ($+c$ plane); (b) N polar (000 $\bar{1}$) surface ($-c$ plane); (c) nonpolar (10 $\bar{1}0$) surface (m plane); (d) nonpolar (11 $\bar{2}0$) surface (a plane). See text for an explanation of the notations for different structures. In (c), the two lines for IPS and ideal surfaces almost overlap because the difference between their energies is very small.

function of Al chemical potential using the following formula:²⁴

$$\Delta E^f(\mu_{\text{Al}}) = E_{\text{surf}}^{\text{tot}} - E_{\text{ideal}}^{\text{tot}} - (n_{\text{Al}} - n_{\text{N}})\mu_{\text{Al}} - n_{\text{N}}\mu_{\text{AlN}}^{\text{bulk}}, \quad (1)$$

in which $E_{\text{surf}}^{\text{tot}}$ and $E_{\text{ideal}}^{\text{tot}}$ are the total energies of the reconstructed and the relaxed ideal (unreconstructed) surfaces. The latter is used as the reference, and this reference is different for each surface orientation. n_{Al} and n_{N} are the numbers of the Al and the N atoms added to (positive) or subtracted from (negative) the ideal surface. We assume that all species are in equilibrium with AlN. Therefore, the chemical potentials of Al and N are not independent and are related through the expression

$$\mu_{\text{Al}} + \mu_{\text{N}} = \mu_{\text{AlN}}^{\text{bulk}} = \mu_{\text{Al}}^{\text{bulk}} + \mu_{\text{N}_2} + \Delta H_{\text{AlN}}^f, \quad (2)$$

in which ΔH_{AlN}^f is the formation enthalpy of AlN. For convenience, we reference all the chemical potentials to the energy (per atom) of bulk Al $\mu_{\text{Al}}^{\text{bulk}}$ and of the nitrogen molecule μ_{N_2} . Our calculations using the PBE functional found a value of 2.86 eV for ΔH_{AlN}^f indicating that the chemical potential of Al ranges from 0 eV for Al-rich conditions to -2.86 eV for Al-poor conditions.

III. RESULTS AND DISCUSSIONS

A. Surface reconstructions

The formation energies of selected reconstructions on AlN polar and nonpolar surfaces and their dependence on the Al chemical potential are presented in Fig. 1. The structures of selected reconstructions are shown in Fig. 2. For the (0001) surface, nine possible reconstructions were optimized by use of GGA. In increasing order of formation energy under Al-

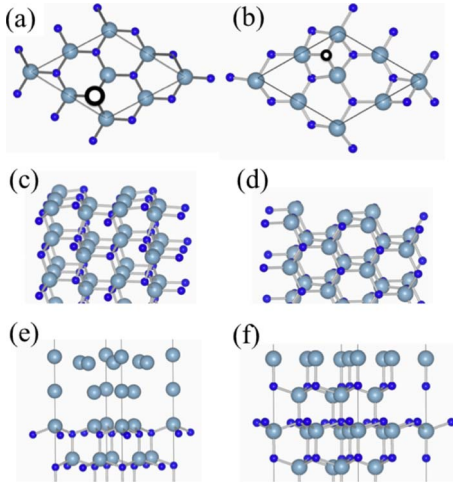


FIG. 2. (Color online) Structures of selected AlN surface reconstructions. (a) Al adatom at $T4$ site on (0001) surface (top view); (b) N adatom at $H3$ site on $(000\bar{1})$ surface (top view); (c) ideal $(10\bar{1}0)$ surface (side view); (d) ideal $(11\bar{2}0)$ surface (tilted side view); (e) Al LCB on (0001) surface (tilted side view); (f) Al top adlayer on $(000\bar{1})$ surface (side view). The black circles in (a) and (b) show the adatoms on $T4$ and $H3$ sites, respectively.

poor conditions [points on the left ordinate axis in Fig. 1(a)], they are (1) N adsorption at $H3$ site (N_{H3}), (2) single Al vacancy (V_{Al}), (3) ideal surface (all the ideal surfaces are relaxed), (4) Al adsorption at $T4$ site (Al_{T4}), (5) N vacancy (V_N), (6) Al substitution of N at subsurface layer (Al_N), (7) monolayer (ML) of Al adsorption at $T4$ site (Al_{T4} layer), (8) Al laterally contracted monolayer (LCM), and (9) Al laterally contracted bilayer (LCB).

$T4$ and $H3$ denote the two high-symmetry adsorbate sites: the $T4$ site [see Fig. 2(a)] is on top of a second layer atom and the $H3$ site [see Fig. 2(b)] is the hollow site. The ideal surface consists of only Al atoms, each of which bonds with three N in the sublayer below the surface layer. Several other reconstructions, including N adsorption at $T4$ site, Al vacancy plus N adsorption at $H3$, and Al adsorption at $H3$ site, were also calculated but not shown in the figure. None of them become stable within the allowed chemical-potential region.

In Fig. 1(b), the reconstructions calculated for the $000\bar{1}$ surface are (also in increasing order of formation energy under Al-poor conditions) (1) Al adsorption at $H3$ site (Al_{H3}), (2) Al adsorption at $T4$ site (Al_{T4}), (3) ideal surface, (4) Al monolayer with Al atoms on top of N (Al_{top} layer), and (7) Al bilayer. The ideal surface consists of only N atoms that bond with three Al atoms in the sublayer. We also studied the N vacancy, the Al monolayer with Al occupying $T4$ sites, and the Al monolayer with Al occupying $H3$ sites and found their formation energies higher than those of Al_{H3} and Al_{top} monolayer reconstructions. Most of the reconstructions, except for the LCB on the (0001) surface, are modeled using (2×2) surface unit cells. The LCB reconstruction is modeled using a $(\sqrt{3} \times \sqrt{3})$ surface unit cell.⁸

Formation energies for nonpolar surfaces are presented in Figs. 1(c) and 1(d). For the surface, the reconstructions stud-

ied in the present work include (1) ideal surface (Al-N dimer), (2) inverted polarity structure (IPS), (3) N-N dimer, (4) two-Al-atom (2Al) adsorption, (5) Al-Al dimer, and (6) Al bilayer. Finally, the reconstructions for the surface include (1) ideal surface, (2) N vacancy (V_N), (3) Al substitution of N (Al_N), (4) two-Al substitution of N ($2Al_N$), and (5) Al bilayer on top of two-Al substitution of N.

1. (0001) surfaces

Our calculations show that the surface reconstruction strongly depends on the chemical condition of the environment. As shown in Fig. 1(a), the surface is stable in the N_{H3} reconstruction [Fig. 2(b)] over a wide range of chemical potentials, ranging from Al poor ($\mu_{Al} = -2.86$ eV) up to fairly Al rich ($\mu_{Al} = -0.51$ eV). The formation energy of this reconstruction is 2.4 eV per (2×2) under Al-poor conditions. As the Al chemical potential increases further, the surface changes from N adsorption to Al adsorption [Al_{T4} , Fig. 2(a)]. The corresponding formation energy is -0.58 eV per (2×2) under Al-rich conditions ($\mu_{Al} = 0$ eV). The site preference also changes from $H3$ to $T4$. This is because an adatom at a $T4$ site strongly interacts with the N atom below the Al layer, which is attractive to Al atoms but repulsive to N atoms.

Under highly Al-rich conditions, monolayers (LCM) or bilayers (LCB) of Al start to form on the surface. Both structures have been studied in previous work.⁸ Figure 2(e) shows the structure of the LCB. Our calculations show a transition directly from the Al-adatom structure to the LCB at an Al chemical potential of about -0.1 eV. This result differs from a previous study which found a region of stability for the LCM structure.⁸ In that study, the LCB structure was always higher in energy than the LCM until Al reached the chemical potential of bulk Al metal (i.e., $\mu_{Al} = 0$). Under this condition, the formation energy of the LCB is -0.94 eV per $(\sqrt{3} \times \sqrt{3})$ cell, which is equivalent to -1.25 eV per (2×2) cell.

2. $(000\bar{1})$ surfaces

Turning now to the $(000\bar{1})$ (N polar) surface, we find that N adsorption on the surface is never favorable, in contrast to the (0001) surface where it is favorable under Al-poor (N-rich) conditions. On the $(000\bar{1})$ surface, Al adsorption (in the form of adatoms or adlayers) is favored throughout the chemical-potential range. We find a transition point from adatom to adlayer at about -0.5 eV. The Al adatom favors the $H3$ site due to the repulsive interaction with an Al atom in the layer below the N layer in the case of $T4$. The formation energy of adatoms changes from -2.19 eV under Al-poor conditions ($\mu_{Al} = -2.86$ eV) to -5.05 eV under Al-rich conditions ($\mu_{Al} = 0$ eV). The formation energy of the Al_{top} adlayer is -6.53 eV at the Al-rich limit, and the formation energy of the Al bilayer is about 0.4 eV higher than that.

We note that the adlayer structure for the N polar surface is very different from the adlayer on the Al polar surface. We found that bilayers always have higher energy than monolayers on the $(000\bar{1})$ surface. Al atoms in the monolayer located right on top of N atoms form strong Al-N bonds [Fig. 2(f)].

It has been recognized that the growth of group-III nitrides under highly cation-rich conditions can help to promote a smooth morphology at the surface.⁴³ This was attributed, based on a theoretical model, to the formation of cation bilayers that can lead to a more efficient diffusion channel at the surface during molecular-beam epitaxy growth.⁴⁴ Our calculations show that, because of the lack of bilayers, this mechanism does not apply to N-polar AlN surfaces, which indicates that the increase in the Al flux might not improve the morphology for N-polar surface growth in the way that metallic bilayers do for GaN grown in the (0001) orientation.^{44,45} Our previous calculations for GaN and InN also found a lower formation energy for a cation monolayer.²⁴ It has been shown experimentally that although increasing the Ga/N flux ratio can improve the morphology of the N-polar GaN surface,⁴⁶ Ga droplets will start to form when excess Ga at the surface is beyond 1 ML.⁴⁷ For AlN, high-quality N-polar AlN layers were grown by optimizing the growth temperature, but the effects of Al/N flux ratio were not addressed.⁴⁸ Our calculations suggest that an Al monolayer forms during the growth of N-polar AlN with higher Al/N ratios, similar to the case of N-polar GaN, but we note that the energy differences between the monolayer and the bilayer are noticeably larger for AlN.

3. (10 $\bar{1}0$) surfaces

Compared to the polar surfaces, we find that the nonpolar surfaces are relatively insensitive to variations in the Al chemical potential. For (10 $\bar{1}0$), the ideal surface is stable over a very large range of μ_{Al} . Its structure is shown in Fig. 2(c). The stability of the ideal surface is due to the presence of Al-N pairs (dimers) at the surface and the fact that the excess charge in the high-energy Al dangling bonds (DBs) can be transferred to the low-energy N DBs. This charge redistribution changes the bonding features of each atom, making the N atom more like and the Al atom more s^2p^3 -like. Consistent with this bonding picture, the N atoms on the relaxed (10 $\bar{1}0$) surface move outward and the Al atoms move inward.

In previous work,²⁴ an interesting reconstruction was found for GaN and InN surfaces in which the polarity of the bonds in the outermost layer is inverted. The formation energies of these IPSs are only 0.06 and 0.10 eV higher per (1 \times 1) cell than the ideal surfaces for GaN and InN, respectively. We examined this structure for AlN and found that the formation energy of IPS is, again, higher than the ideal surface, but with an energy difference of only 0.05 eV per (1 \times 1) cell, indicating the possibility of forming domains with locally inverted polarity in AlN samples grown along the (10 $\bar{1}0$) orientation.

For $\mu_{\text{Al}}=0$ eV, the formation energies for the 2Al structure (i.e., a single adlayer) and Al bilayer structures are -0.63 and -0.60 eV, respectively, indicating that a single Al adlayer can form on the (10 $\bar{1}0$) surface under these Al-rich conditions. The transition chemical potential from the ideal surface to the single adlayer reconstruction is at -0.33 eV. The bilayer reconstructions are higher in energy, but the energy difference becomes quite small under highly Al-rich

conditions (0.03 eV at $\mu_{\text{Al}}=0$ eV), and therefore the formation of such bilayers cannot be excluded. Because of the difference in lattice constant between AlN and Al, Al bilayers are usually contracted in volume, resulting in a lowering of their formation energy, a feature that is not included in our bilayer models for nonpolar surfaces. Therefore, we cannot conclusively state whether or not bilayer reconstructions form on these nonpolar surfaces.

4. (11 $\bar{2}0$) surfaces

For (11 $\bar{2}0$), the ideal surface is stable throughout the chemical-potential range, again due to the stability of Al-N dimers that are naturally present on this surface. Its structure is shown in Fig. 2(d). However, under extreme Al-rich conditions ($\mu_{\text{Al}}=0$), the energy difference between the ideal surface and the Al bilayer structure is less than 0.1 eV. Again, the formation of bilayers under these conditions cannot be excluded.

5. Electron-counting rule

When searching for stable surface reconstructions, the electron-counting rule is a good guide.⁴⁹ It states that the number of electrons at the surface should be such that all surface bonding states and all anion (N) DB states are occupied and that all cation (Al) DB states are empty. The rule is motivated by the fact that anion DB states usually occur low in the gap, near the valence-band maximum (VBM) (recall that in compound semiconductors the character of the VBM is mainly anion derived) and that cation DB states usually occur high in the gap, near the CBM (which is typically mainly cation derived). We indeed verified that all the reconstructions that are found to be stable in our study satisfy the electron-counting rule, except for adlayer structures. The Al adlayer structures are metallic, a case to which the electron counting does not apply.

As an example, the ideal (2 \times 2) (0001) surface contains four Al atoms and each of the atoms has one cation DB containing 3/4 electron. Therefore there are three electrons occupying four cation DBs. This is unstable according to the electron-counting rule. The $\text{N}_{\text{H}3}$ adatom reconstruction has three Al-N bonds, one Al DB, and one N DB. Because N has five electrons, the total number of electrons is $5+3=8$, which is just right to fill the N DB states and Al-N bonding states. Similarly, the $\text{Al}_{\text{T}4}$ reconstruction has six electrons, which fill three Al-Al bonding states and leave the two Al DB states empty. Therefore, both $\text{N}_{\text{H}3}$ and $\text{Al}_{\text{T}4}$ satisfy the electron-counting rule.

6. General trends

Previous studies^{20,24} as well as the current work indicate that the surface reconstructions of group-III nitrides depend on the chemical conditions. Under cation-poor conditions, N adsorption at the $\text{H}3$ site is the most stable configuration for the (0001) surface. A transition to cation adsorption happens at $\mu_{\text{Al}}=-0.51$ eV. Under even more highly cation-rich conditions, the LCB becomes the most favored surface structure. For the (000 $\bar{1}$) surface, N adsorption does not occur and the

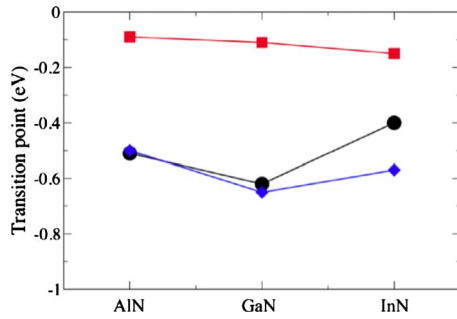


FIG. 3. (Color online) Transition points (values of the cation chemical potential for which transitions between different reconstructions occur) for group-III nitride semiconductors, as explained in the text. Filled circles represent the nitrogen adatom to cation adatom transition on (0001), squares represent the adatom to LCB transition on (0001), and diamonds represent the cation adatom to monolayer transition on (000 $\bar{1}$).

only transition occurs between cation adsorption and a cation monolayer at $\mu_{\text{Al}} \approx -0.5$ eV. It is instructive to compare the transition points (cation chemical-potential values for which transition between different reconstructions occur) for AlN, GaN, and InN. To eliminate possible discrepancies due to the use of different exchange-correlation functionals in previous work, we recalculated the transition points for GaN and InN using the PBE functional.

Figure 3 presents the transition points for three transitions on AlN, GaN, and InN polar surfaces: nitrogen adatom to cation adatom on (0001), cation adatom to LCB on (0001), and cation adatom to cation monolayer on (000 $\bar{1}$). Because of the low formation enthalpy of InN, the In chemical-potential window is very narrow and the transitions between the N adatom and In adatom reconstructions for (0001) and between In adatom and In monolayer for (000 $\bar{1}$) surface are outside this window. However, for the purpose of comparison, we extrapolate those surface energies beyond the limits of the In chemical potential to obtain the transition points. It is interesting to note that, although the three nitrides have very different formation enthalpies, the transitions between different surface structures happen at very similar cation chemical potentials.

B. Electronic structure

The periodic crystal lattice of a semiconductor is discontinued at a surface, and the resulting broken bonds typically give rise to surface states. If these surface states occur within the band gap of the semiconductor, they may have strong effects on the electronic properties of the material. For example, a surface donor state in the band gap can pin the Fermi level for *p*-type material. Note that empty surface states above the CBM, or filled surface states below the VBM, are typically considered innocuous.

1. (0001) surfaces

Figure 4 presents the band structures of selected reconstructions on polar and nonpolar surfaces. The Al_{T4} recon-

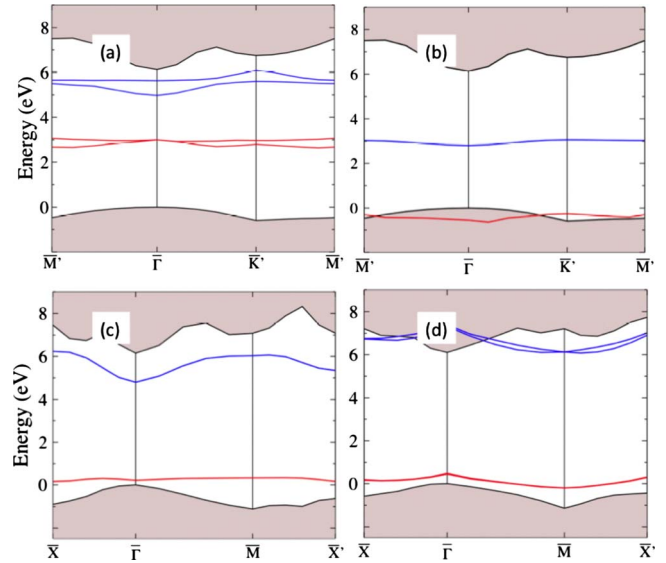


FIG. 4. (Color online) Calculated band structures of selected surface reconstructions on polar and nonpolar surfaces. (a) Al at T_4 site on Al polar (0001) surface; (b) Al adsorption at H_3 site on N polar (000 $\bar{1}$) surface; (c) ideal (10 $\bar{1}0$) surface; (d) ideal (11 $\bar{2}0$) surface. The red lines (in the lower part of the gap) show the occupied surface states, and the blue lines (in the upper part of the gap) show the unoccupied surface states. Shaded areas indicate the projected band structure of bulk AlN.

struction on the surface consists of Al-Al bonds and Al DBs at the surface that give rise to two sets of states in the gap. The lower set corresponds to Al-Al bonding states and is completely filled. It occurs at 3.13 eV above the VBM at the $\bar{\Gamma}$ point. The upper set corresponds to the Al DB states and is empty. The two bands in the upper set are nondegenerate at the $\bar{\Gamma}$ point, with the lower one occurring at 1.16 eV below the CBM. In an *n*-type AlN sample, this level would be responsible for Fermi-level pinning. Our result is in excellent comparison with recent *in situ* x-ray photoemission spectroscopy measurements for as-grown AlGaIn samples, which found that the Fermi level was pinned at 1.2 eV below the CBM for AlN.⁵⁰ The two bands in the upper part of the gap are a mixture of the two Al DB states, with the lower one mainly consisting of the DB on the Al adatom and the upper one mainly consisting of the DB on the Al atom in the surface layer. A similar band structure was found for the Ga-adatom reconstruction on the GaN surface, in which the Ga DB state can pin the Fermi level of *n*-type GaN at about 0.6 eV below the CBM.²³

The N adatom reconstruction N_{H_3} is stable for the Al polar (0001) surface under Al-poor conditions. It is informative to compare its electronic structure with that of the Al_{T4} reconstruction which occurs under relatively Al-rich conditions. As shown in Fig. 5, the N_{H_3} reconstruction has four surface states in the gap, three of which are filled and one is empty. The lowest two are degenerate at the $\bar{\Gamma}$ point (and almost degenerate over most of the surface Brillouin zone) and occur at about 1 eV above the VBM. They correspond to the Al-N bonding states. The N DB state occurs at about 2.1 eV above the VBM. The relatively high energies for Al-N

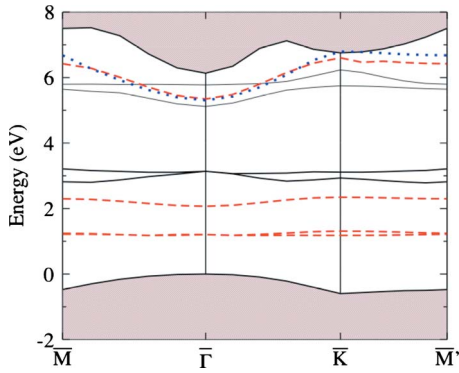


FIG. 5. (Color online) Comparison of band structures of several reconstructions on the Al polar (0001) surface, including Al_{T4} (black solid lines); N_{H3} (red dashed lines); and the hydrogen-passivated ideal surface (blue dotted line). Note the similar positions of the Al-DB-related unoccupied surface states in the upper part of the band gap.

bonding and N DB states correlate with the geometry relaxation of the N atom on the surface. We found that the Al-N-Al angle is close to 90° , consistent with s^2p^3 hybridization. Three Al-N bonds are present, leading to the following three filled states: the filled state corresponding to the N s orbital is located deep inside the valence bands; the two Al-N bonding states that are formed by N p_x and p_y orbitals are higher in energy than those formed by N sp^3 orbitals, and therefore located above the VBM; finally, the N DB state is a N p_z state and is deep in the gap.

In addition, an empty surface state relating to the Al DB occurs at 5.3 eV above VBM. This is close to the position of the Al DB state for the Al_{T4} reconstruction. We find that the position of this Al DB state on the Al polar surface is quite insensitive to the reconstructions. In another example, we performed calculations for a hydrogenated Al polar surface in which three Al DBs are passivated by hydrogen adatoms; the resulting Al-H bonding states are moved away from the gap. This leaves only one surface state in the gap, related to a single DB on an Al surface atom. Its position is also 5.3 eV above the VBM. Coupling between the two Al DBs on the surface causes the shifts of Al DB states in the case of the Al_{T4} reconstruction.

2. (000 $\bar{1}$) surfaces

The Al adatom reconstruction on the (000 $\bar{1}$) surface, which is stable over a very wide range of chemical potentials [see Fig. 1(b)], contains both Al and N DBs. Figure 4(b) shows that the N DB state is filled and occurs slightly below the VBM. The Al DB state is empty and occurs at 2.8 eV above the VBM. The Al-N bonding states are below the VBM. Compared with the Al-polar (0001) surface, the N-polar (000 $\bar{1}$) surface thus behaves quite differently. It does not have a filled state in the gap, and hence it cannot pin the Fermi level for p -type material. The empty DB state occurs just slightly below midgap and will thus lead to Fermi-level pinning for n -type material at an energy much lower in the gap compared to (0001), where the empty DB states occur within 1 eV of the CBM.

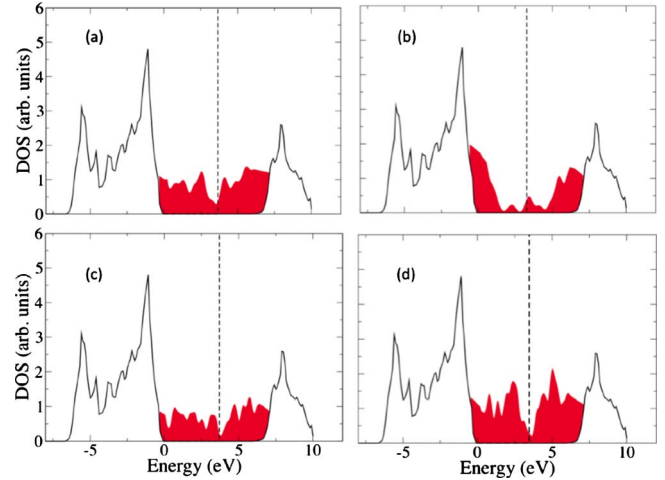


FIG. 6. (Color online) Calculated DOS of Al-wetted surfaces. (a) Laterally contracted bilayer on the Al polar (0001) surface; (b) Al monolayer on the N polar (000 $\bar{1}$) surface; (c) Al bilayer on the (10 $\bar{1}0$) surface; (d) Al monolayer on top of 2Al substitution of N on the (11 $\bar{2}0$) surface. The solid black lines show the bulk DOS, the shaded areas (red) show the DOS arising from surface states, and the vertical dashed lines show the Fermi levels.

3. (10 $\bar{1}0$) and (11 $\bar{2}0$) surfaces

The (10 $\bar{1}0$) and the (11 $\bar{2}0$) surfaces have similar features in their electronic structures. They both contain Al DB states that are close to the CBM and N DB states that are close to the VBM. At the $\bar{\Gamma}$ point, the N DB state is about 0.2 eV above the VBM for the (10 $\bar{1}0$) surface and about 0.4 eV above the VBM for the (11 $\bar{2}0$) surface. This indicates that the Fermi level on nonpolar surfaces of p -type material would occur close to the VBM. The Al DB state is located at 4.8 eV above the VBM for the (10 $\bar{1}0$) surface, indicating a similar surface band bending and Fermi-level pinning as on the Al polar (0001) surface. On the other hand, the Al DB state lies above the CBM on the (11 $\bar{2}0$) surface and will have no effects on the electronic properties of the material.

4. Metallic monolayers or bilayers

Under Al-rich conditions, most of the AlN surfaces can accommodate single or double Al adlayers. These layers are metallic and have strong effects on the electronic properties of the surface. In the case of these adlayers, surface band structures are less informative because usually multiple highly dispersive bands occur throughout the band gap; to examine the effects, it is more informative to calculate the density of states (DOS) which also shows the resulting Fermi-level position. DOS plots for selected adlayer reconstructions on polar and nonpolar surfaces are presented in Fig. 6. The DOS plots show that all the adlayers are metallic. Their Fermi levels are located at similar positions in the gap: measured from the VBM, the Fermi levels are at 3.66, 3.27, 3.71, and 3.30 eV for the (0001) LCB, (000 $\bar{1}$) monolayer, (10 $\bar{1}0$) bilayer, and (11 $\bar{2}0$) monolayer, respectively. The

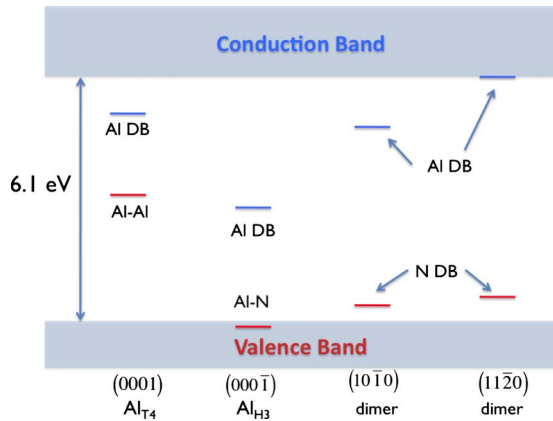


FIG. 7. (Color online) Surface states in the band gap for selected reconstructions on AlN polar and nonpolar surfaces. The surface states of different surface reconstructions are aligned to the VBM of the bulk.

similarity in Fermi-level position of the Al adlayers can be understood by the lineup of AlN bands and the Fermi level of Al metal. The position of the VBM relative to the vacuum level, i.e., the ionization potential of AlN, is about 7.5 eV.⁵¹ The work function of Al metal is about 4.2 eV.⁵² Therefore, the Fermi level of Al metal is expected to be located at around 3.3 eV above the VBM of AlN.

5. Trends

The positions of the surface states in the band gap are consistent with the origin of the electron-counting rule. As summarized in Fig. 7, surface states associated with a N DB and with Al-N bonding states occur in the lower half of the band gap, quite close to the VBM. In contrast, Al DB states occur in the upper half of the gap. Al-Al bonds give rise to states around midgap. Because of these positions, it is favorable to occupy N DBs and Al-N bonding states with electrons, while Al DB states are better left empty.

The positions of the various types of surface states in the band gap show similar trends across the different nitride semiconductors, as revealed in Fig. 8. Note that the In-In bonding state follows the general trend, but because of the low energy of the CBM at Γ this occupied state now lies above CBM of InN. As noted in Ref. 21 this explains the universally observed occurrence of an electron accumulation layer on polar InN surfaces. This result for InN is actually consistent with the general trend that the III-III bonding-state position in the gap is close to the Fermi-level position of cation adlayers. The latter can be lined up with the band structure of the nitride, as noted above in the case of AlN. In the case of InN, the ionization potential is about 6.2 eV,⁵¹ whereas the work function of In metal is about 4.2 eV.⁵² Given the band-gap value of 0.7 eV,^{40,53-56} the Fermi level of In metal ends up at about 1.3 eV above the InN CBM.

6. Relevance for devices

Besides pinning the Fermi level, the surface states of nitride semiconductors may also play an important role in AlGaN/GaN HEMT devices. Although the presence of a

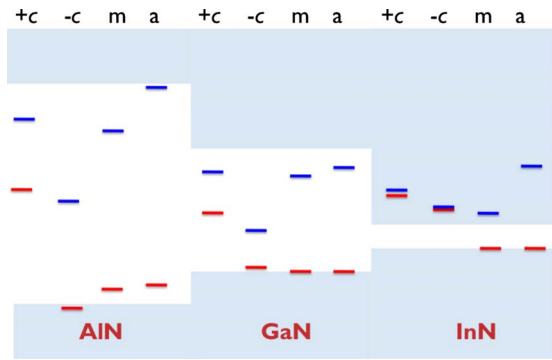


FIG. 8. (Color online) Overview of surface states on AlN, GaN, and InN surfaces. +c and -c denote the cation and the nitrogen polar surfaces, respectively. The selected reconstructions and the presented surface states are the same as in Fig. 7. The AlN/GaN and GaN/InN band offsets are set as 0.85 and 0.5 eV (Ref. 57). The results for GaN and InN are taken from previous work (Refs. 21 and 22). Each surface has two states. The upper one (blue) is unoccupied and the lower one (red) is occupied.

2DEG at the interface between GaN and AlGaN has been observed for more than a decade, its origin is still not completely understood. Ibbetson *et al.*¹³ proposed that the electrons in the 2DEG originate from surface states on the Al-GaN surface, a mechanism that is now widely accepted (see Fig. 9). A number of experimental studies have shown that these surface donor states need to be located in the upper part of the gap, specifically at about 1.65 eV below the CBM for a 34% Al composition AlGaN sample.¹³ By applying linear interpolation, the corresponding surface state should be located at about 2.2 eV below the CBM on the pure AlN (0001) surface. It would be of interest to identify any surface reconstructions that give rise to such a surface donor state in the upper part of the gap.

Our investigations have made clear that surface states on the bare AlN surface are related to either a DB (Al or N) or a bonding state (Al-Al or Al-N). According to our calculated results, Al-N bonding and N DB states tend to be close to the VBM or even below it. These states are occupied with electrons and could hence act as donor states, but they are too low in energy to be consistent with the experimental observations on the 2DEG at AlGaN/GaN interfaces. Al DB states, on the other hand, do occur in the upper half of the gap. However, the Al DB states in stable reconstructions are all empty and can therefore not serve as surface donor states (i.e., as a source of electrons). We did find that the Al adlayer reconstruction is metallic and has a Fermi level at about

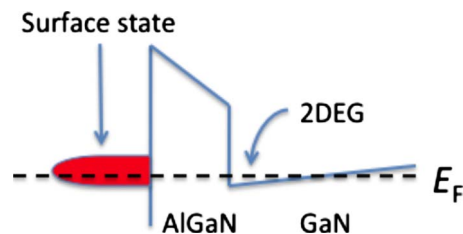


FIG. 9. (Color online) Origin of the two-dimensional electron gas at an AlGaN/GaN interface.

2.54 eV below the CBM. The corresponding states, which occur in highly metal-rich reconstructions, are therefore the primary candidate for surface donors on the bare AlN surface.

We note, however, that when exposed to air most nitride surfaces will not preserve the surface reconstructions corresponding to bare surfaces, but will tend to oxidize. In particular, the metallic adlayer structure that emerged as the best candidate for surface donors will probably be rapidly oxidized in air.^{58,59} Modifications of the atomic and electronic structure of the surface due to oxidation have already been investigated both by experiments^{58,60} and by computations.⁵⁸ We are currently devoting further study to this issue.

IV. CONCLUSIONS

We have studied the stability and the electronic structure of reconstructions on AlN polar and nonpolar surfaces using density-functional methods with both GGA and hybrid functionals. The dependence of surface reconstructions on the chemical potentials of Al and N was systematically investigated. Transitions between different reconstructions were found to occur at similar values of cation chemical potentials across the group-III nitrides. Metallic Al adlayers are likely

to occur on both polar and nonpolar surfaces under highly Al-rich conditions, producing Fermi-level positions just above midgap, consistent with the alignment of the Fermi level of Al metal in the AlN gap.

The electronic structure of all surfaces is consistent with the electron-counting rule. Bonding states, such as Al-Al and Al-N states, as well as N DB states have energies in the lower part of the band gap and are fully occupied, whereas Al DB states are found in the upper part of the gap and are unoccupied. These general trends, which are fully backed up by our first-principles calculations, indicate that surface donor states on clean AlGaN surfaces are unlikely to be the source of electrons in the 2DEG in AlGaN/GaN HEMTs.

ACKNOWLEDGMENTS

This work was supported by the Office of Naval Research under Grant No. N00014-08-1-0095, monitored by P. Maki. It made use of NSF-funded TeraGrid resources, especially Ranger, maintained by the Texas Advanced Computing Center under Grant No. DMR070072N. We thank G. Kresse for providing an unreleased version of the VASP code.⁶¹ We also would like to thank Patrick Rinke and Poul G. Moses for inspiring discussions.

-
- ¹L. Shen, R. Coffie, D. Buttari, S. Heikman, A. Chakraborty, A. Chini, S. Keller, S. P. DenBaars, and U. K. Mishra, *J. Electron. Mater.* **33**, 422 (2004).
- ²S. Rajan, P. Waltereit, C. Poblenz, S. J. Heikman, D. S. Green, J. S. Speck, and U. K. Mishra, *IEEE Electron Device Lett.* **25**, 247 (2004).
- ³A. J. Fischer, A. A. Allerman, M. H. Crawford, K. H. A. Bogart, S. R. Lee, R. J. Kaplar, W. W. Chow, S. R. Kurtz, K. W. Fullmer, and J. J. Figiel, *Appl. Phys. Lett.* **84**, 3394 (2004).
- ⁴K. Iida, T. Kawashima, A. Miyazaki, H. Kasugai, S. Mishima, A. Honshio, Y. Miyake, M. Iwaya, S. Kamiyama, H. Amano, and I. Akasaki, *J. Cryst. Growth* **272**, 270 (2004).
- ⁵C. G. Moe, H. Masui, M. C. Schmidt, L. K. Shen, B. Moran, S. Newman, K. Vampola, T. Mates, S. Keller, J. S. Speck, S. P. DenBaars, C. Hussey, and D. Emerson, *Jpn. J. Appl. Phys., Part 2* **44**, L502 (2005).
- ⁶C. S. Davis, S. V. Novikov, T. S. Cheng, R. P. Campion, and C. T. Foxon, *J. Cryst. Growth* **226**, 203 (2001).
- ⁷R. M. Feenstra, Y. Dong, C. D. Lee, and J. E. Northrup, *J. Vac. Sci. Technol. B* **23**, 1174 (2005).
- ⁸C. D. Lee, Y. Dong, R. M. Feenstra, J. E. Northrup, and J. Neugebauer, *Phys. Rev. B* **68**, 205317 (2003).
- ⁹H. Masui, M. Schmidt, N. Fellows, H. Yamada, K. Iso, J. S. Speck, S. Nakamura, and S. P. DenBaars, *Phys. Status Solidi A* **206**, 203 (2009).
- ¹⁰B. Imer, M. Schmidt, B. Haskell, S. Rajan, B. Zhong, K. Kim, F. Wu, T. Mates, S. Keller, U. K. Mishra, S. Nakamura, J. S. Speck, and S. P. DenBaars, *Phys. Status Solidi A* **205**, 1705 (2008).
- ¹¹H. Masui, M. C. Schmidt, A. Chakraborty, S. Nakamura, and S. P. DenBaars, *Jpn. J. Appl. Phys., Part 1* **45**, 7661 (2006).
- ¹²A. Tyagi, Y. D. Lin, D. A. Cohen, M. Saito, K. Fujito, J. S. Speck, S. P. DenBaars, and S. Nakamura, *Appl. Phys. Express* **1**, 091103 (2008).
- ¹³J. P. Ibbetson, P. T. Fini, K. D. Ness, S. P. DenBaars, J. S. Speck, and U. K. Mishra, *Appl. Phys. Lett.* **77**, 250 (2000).
- ¹⁴S. Keller, S. Heikman, L. Shen, I. P. Smorchkova, S. P. DenBaars, and U. K. Mishra, *Appl. Phys. Lett.* **80**, 4387 (2002).
- ¹⁵I. P. Smorchkova, L. Chen, T. Mates, L. Shen, S. Heikman, B. Moran, S. Keller, S. P. DenBaars, J. S. Speck, and U. K. Mishra, *J. Appl. Phys.* **90**, 5196 (2001).
- ¹⁶G. Koley and M. G. Spencer, *Appl. Phys. Lett.* **86**, 042107 (2005).
- ¹⁷J. Fritsch, O. F. Sankey, K. E. Schmidt, and J. B. Page, *Phys. Rev. B* **57**, 15360 (1998).
- ¹⁸K. Kadas, S. Alvarez, E. Ruiz, and P. Alemany, *Surf. Sci.* **355**, 167 (1996).
- ¹⁹M. E. Mora-Ramos and V. R. Velasco, *Surf. Sci.* **600**, 2868 (2006).
- ²⁰J. E. Northrup, R. DiFelice, and J. Neugebauer, *Phys. Rev. B* **55**, 13878 (1997).
- ²¹D. Segev and C. G. Van de Walle, *EPL* **76**, 305 (2006).
- ²²C. G. Van de Walle and D. Segev, *J. Appl. Phys.* **101**, 081704 (2007).
- ²³D. Segev and C. G. Van de Walle, *J. Cryst. Growth* **300**, 199 (2007).
- ²⁴D. Segev and C. G. Van de Walle, *Surf. Sci.* **601**, L15 (2007).
- ²⁵D. Segev, A. Janotti, and C. G. Van de Walle, *Phys. Rev. B* **75**, 035201 (2007).
- ²⁶P. Hohenberg and W. Kohn, *Phys. Rev.* **136**, B864 (1964).
- ²⁷W. Kohn and L. J. Sham, *Phys. Rev.* **140**, A1133 (1965).
- ²⁸N. E. Christensen, *Phys. Rev. B* **30**, 5753 (1984).

- ²⁹Y.-S. Kim, K. Hummer, and G. Kresse, *Phys. Rev. B* **80**, 035203 (2009).
- ³⁰J. P. Perdew, K. Burke, and M. Ernzerhof, *Phys. Rev. Lett.* **77**, 3865 (1996).
- ³¹J. Heyd, G. E. Scuseria, and M. Ernzerhof, *J. Chem. Phys.* **118**, 8207 (2003).
- ³²J. Heyd and G. E. Scuseria, *J. Chem. Phys.* **121**, 1187 (2004).
- ³³J. Heyd, G. E. Scuseria, and M. Ernzerhof, *J. Chem. Phys.* **124**, 219906 (2006).
- ³⁴P. E. Blochl, *Phys. Rev. B* **50**, 17953 (1994).
- ³⁵G. Kresse and D. Joubert, *Phys. Rev. B* **59**, 1758 (1999).
- ³⁶G. Kresse and J. Hafner, *Phys. Rev. B* **47**, 558 (1993).
- ³⁷G. Kresse and J. Furthmuller, *Phys. Rev. B* **54**, 11169 (1996).
- ³⁸D. Brunner, H. Angerer, E. Bustarret, F. Freudenberger, R. Hopler, R. Dimitrov, O. Ambacher, and M. Stutzmann, *J. Appl. Phys.* **82**, 5090 (1997).
- ³⁹J. Li, K. B. Nam, M. L. Nakarmi, J. Y. Lin, H. X. Jiang, P. Carrier, and S. H. Wei, *Appl. Phys. Lett.* **83**, 5163 (2003).
- ⁴⁰P. Rinke, M. Winkelkemper, A. Qteish, D. Bimberg, J. Neugebauer, and M. Scheffler, *Phys. Rev. B* **77**, 075202 (2008).
- ⁴¹H. Schulz and K. H. Thiemann, *Solid State Commun.* **23**, 815 (1977).
- ⁴²W. M. Yim, E. J. Stofko, P. J. Zanzucchi, J. I. Pankove, M. Ettenber, and S. L. Gilbert, *J. Appl. Phys.* **44**, 292 (1973).
- ⁴³B. Heying, I. Smorchkova, C. Poblentz, C. Elsass, P. Fini, S. Den Baars, U. Mishra, and J. S. Speck, *Appl. Phys. Lett.* **77**, 2885 (2000).
- ⁴⁴J. Neugebauer, T. K. Zywiets, M. Scheffler, J. E. Northrup, H. Chen, and R. M. Feenstra, *Phys. Rev. Lett.* **90**, 056101 (2003).
- ⁴⁵G. Koblmuller, J. Brown, R. Averbeck, H. Riechert, P. Pongratz, and J. S. Speck, *Appl. Phys. Lett.* **86**, 041908 (2005).
- ⁴⁶S. Rajan, M. Wong, Y. Fu, F. Wu, J. S. Speck, and U. K. Mishra, *Jpn. J. Appl. Phys., Part 2* **44**, L1478 (2005).
- ⁴⁷E. Monroy, E. Sarigiannidou, F. Fossard, N. Gogneau, E. Bellet-Amalric, J. L. Rouviere, S. Monnoye, H. Mank, and B. Daudin, *Appl. Phys. Lett.* **84**, 3684 (2004).
- ⁴⁸S. Dasgupta, F. Wu, J. S. Speck, and U. K. Mishra, *Appl. Phys. Lett.* **94**, 151906 (2009).
- ⁴⁹M. D. Pashley, *Phys. Rev. B* **40**, 10481 (1989).
- ⁵⁰A. Rizzi, M. Kocan, J. Malindretos, A. Schildknecht, N. Teofelov, K. Thonke, and R. Sauer, *Appl. Phys. A: Mater. Sci. Process.* **87**, 505 (2007).
- ⁵¹C. G. Van de Walle and J. Neugebauer, *Nature (London)* **423**, 626 (2003).
- ⁵²*CRC Handbook of Chemistry and Physics*, 89th ed. (Internet version), edited by David R. Lide (CRC Press/Taylor and Francis, Boca Raton, FL, 2009).
- ⁵³V. Y. Davydov, A. A. Klochikhin, R. P. Seisyan, V. V. Emtsev, S. V. Ivanov, F. Bechstedt, J. Furthmuller, H. Harima, V. Mudryi, J. Aderhold, O. Semchinova, and J. Graul, *Phys. Status Solidi B* **229**, R1 (2002).
- ⁵⁴J. Wu, W. Walukiewicz, K. M. Yu, J. W. Ager, E. E. Haller, H. Lu, W. J. Schaff, Y. Saito, and Y. Nanishi, *Appl. Phys. Lett.* **80**, 3967 (2002).
- ⁵⁵Y. Nanishi, Y. Saito, and T. Yamaguchi, *Jpn. J. Appl. Phys., Part 1* **42**, 2549 (2003).
- ⁵⁶P. Rinke, M. Scheffler, A. Qteish, M. Winkelkemper, D. Bimberg, and J. Neugebauer, *Appl. Phys. Lett.* **89**, 161919 (2006).
- ⁵⁷I. Vurgaftman and J. R. Meyer, *J. Appl. Phys.* **94**, 3675 (2003).
- ⁵⁸Y. Dong, R. M. Feenstra, and J. E. Northrup, *J. Vac. Sci. Technol. B* **24**, 2080 (2006).
- ⁵⁹M. Kocan, A. Rizzi, H. Luth, S. Keller, and U. K. Mishra, *Phys. Status Solidi B* **234**, 773 (2002).
- ⁶⁰Y. Dong, R. M. Feenstra, and J. E. Northrup, *Appl. Phys. Lett.* **89**, 171920 (2006).
- ⁶¹VASP 5.1, cms.mpi.univie.ac.at/vasp/